Pergamon

Int. J. Solids Structures Vol. 35, Nos 34–35, pp. 4597–4617, 1998

Printed in Great Britain
0020-7683/98/$—see front matter

PII: S0020-7683(98)00086-9

ON THEORETICAL AND NUMERICAL METHODS IN THE THEORY OF POROUS MEDIA BASED ON POLAR AND NON-POLAR ELASTO-PLASTIC SOLID MATERIALS†

W. EHLERS‡ and W. VOLK
Institut für Mechanik (Bauwesen), Lehrstuhl II, Universität Stuttgart, Pfaffenwaldring 7, D-70569 Stuttgart, Germany

(*Received* 30 *May* 1997; *in revised form* 2 *February* 1998)

Abstract—The consideration of saturated and non-saturated porous solid materials as for instance soil, concrete, sinter materials, polymeric and metallic foams, temperate ice, living tissues, etc. naturally falls into the category of multiphase materials, which can be described by use of a macroscopic continuum mechanical approach within the well-founded framework of the Theory of Porous Media (TPM). In the present contribution, granular elasto-plastic porous solid skeletons (frictional materials) are taken into consideration, where, regardless of whether or not the solid is fluid-saturated or empty, localization phenomena can occur as a result of local concentrations of plastic strains. As a consequence of localization phenomena, the numerical solution of the governing equations generally reveals an ill-posed problem. In particular, the shear band width strongly depends on the mesh size of the finite element discretization by the fact that each mesh refinement leads to a decrease of the shear band width until one obtains a singular surface.

In the present article, it is shown that the inclusion of fluid-viscosity in the saturated case and the inclusion of micropolar grain rotations both in the saturated and in the non-saturated case leads to a regularization of the shear band problem. On the other hand, the inclusion of micropolar degrees of freedom in the sense of the Cosserat brothers additionally allows for the determination of the local average grain rotations. The numerical examples are solved by use of finite element discretization techniques, where, in particular, the computation of shear band localization phenomena is carried out by the example of the well-known geotechnical slope failure problem and two additional academic problems, which clearly demonstrate the efficiency of the proposed procedure.

1. INTRODUCTION

Basically, the description of saturated, partially saturated and empty porous solid materials as for instance concrete, sinter materials, polymeric and metallic foams, temperate ice, living tissues, etc. can be carried out by use of two generally different strategies. On the other hand, the different materials constituting the porous medium, i.e. porous skeleton and pore content (liquid and/or gas), can be taken into account by a micromechanical approach. In this case, each of the materials can be treated, on its own domain, as a single body as far as the different interaction mechanisms at the internal boundaries are properly taken into consideration. On the other hand, one can prescribe an *a priori* assumption of homogenized substructures and apply the well-founded framework of the Theory of Porous Media (TPM). The TPM approach is based on a macroscopic continuum mechanical description of multiphase materials proceeding from the axioms of the classical theory of mixtures (theory of heterogeneously composed continua with internal constraints) together with the concept of volume fractions. In general, both procedures lead to comparable results, provided that the results of the micromechanical treatment are related to the macroscopic domain by convenient averaging strategies. However, apart from some industrial products, there is no information about the geometry of the internal pore structure of both artificial porous materials (e.g. metallic foams) and natural porous solids (e.g. geomaterials). As a result, one can rather apply a virtual than a real averaging procedure

† Dedicated to Peter Haupt on the occasion of his 60th birthday.

‡ Author to whom correspondence should be addressed. Tel.: 0049 711 685 6345. Fax: 0049 711 685 6347. E-mail: ehlers@mechbau.uni-stuttgart.de

to the microstructure of the considered materials. Furthermore, since there is enough experience on macroscopic testing of porous materials, the present considerations directly proceed from the macroscopic description of multiphase materials given by the framework of the Theory of Porous Media. The fundamentals of Porous Media Theories, the development of general TPM material models, the comparison of the TPM with other approaches to multiphase materials, e.g. the Biot's approach or general averaging theories, as well as recent developments can be taken from the relevant literature. The interested reader is referred, for instance, to the work by Biot (e.g. Biot, 1941, 1956) and the articles by Truesdell and Toupin (1960), Bowen (1976, 1980, 1982), de Boer and Ehlers (1986), de Boer *et al.* (1991), Ehlers (1989, 1993a, b), Haupt (1993), Ehlers and Kubik (1994), Coussy (1995), Ehlers *et al.* (1995) and de Boer (1996).

In the present contribution, polar and non-polar granular elasto-plastic solid skeletons (frictional materials) are taken into consideration, where, in the case of micropolar materials, the additional rotational degrees of freedom are applied in the sense of the Cosserat brothers, cf de Borst (1991, 1993), Steinmann (1994, 1995) or Ehlers and Volk (1997a–c). When the solid is saturated, it is assumed that the pore spaces are filled with a viscous pore-liquid. Mass exchanges between the solid and the liquid materials are excluded and both constituents are assumed to exhibit the property of material incompressibility. This assumption is justified insofar as both the compressibility of the solid material and the compressibility of the pore-liquid are much smaller than the compressibility of the solid skeleton (bulk material). Furthermore, the solid skeleton is assumed to undergo only small deformations (geometrically linear theories), even in the framework of elasto-plastic deformations. However, it may be possible that, in the shear band zone, the accumulated plastic strains exceed the geometrically linear range. On the other hand, this usually happens only in a very small domain and, therefore, does not justify the enormous complexity of the geometrically non-linear elasto-plasticity of micropolar solid materials. Following this, the non-symmetric effective skeleton stress is governed by an extension of the Hookean elasticity model, whereas the couple stress is governed by a similar function of the elastic curvature tensor. In frame of the ideal-plastic approximation, the plastic yield limit is governed by the single-surface yield criterion by Ehlers (1993a, 1995), which, in the present article, is extended by the inclusion of both the non-symmetric part of the effective skeleton stress and the couple stress tensor. Based on the concept of the non-associated plasticity, an additional plastic potential function is introduced to govern the plastic strain rate. Concerning the plastic rate of curvature tensor, it is shown that this quantity can be directly computed from the plastic strain rate by use of the micropolar compatibility condition, which, in the case of elasto-plastic materials, has been firstly presented by the authors (Ehlers and Volk, 1997b).

It is known from various experiments, e.g. from biaxial tests, that porous frictional materials exhibit a distinct dilatant behaviour in the plastic domain. As a result, local softening effects occur even in case of the ideal plasticity concept. Thus, dilatancy leads to a localization of plastic deformations in thin bands of finite width (shear bands). However, it is well known that the width of these bands cannot be computed by use of the standard continuum mechanical description, i.e. by use of the concept of non-polar materials in the non-saturated range. In particular, the finite element solution reveals an ill-posed problem, since the shear band width decreases with each mesh refinement until one obtains (ideally) a singular surface.

In the present article, it is shown that the inclusion of fluid-viscosity in the saturated case and the inclusion of micropolar grain rotations both in the saturated and in the non-saturated case leads to a regularization of the shear band problem. On the other hand, the inclusion of micropolar degrees of freedom additionally allows for the determination of the local average grain rotations. The numerical examples are solved by use of finite element discretization techniques in the spatial domain together with one-step methods in the time domain. In particular, the computation of shear band localization phenomena is carried out by the example of the well-known geotechnical slope failure problem and two additional academic problems (numerical biaxial experiments), which clearly demonstrate the efficiency of the proposed methods.

2. GOVERNING EQUATIONS

2.1. *Kinematics*

By use of the Theory of Porous Media (TPM), fluid-saturated porous solid skeleton materials are considered as a mixture of immiscible constituents φ^α with particles X^α ($\alpha = S$: solid skeleton; $\alpha = F$: pore-fluid). In this framework, empty skeleton materials are treated as a special case of saturated media, where the mechanical effect of the pore content is neglected. In general, at any time t, each spatial point $\mathbf{x}$ of the current configuration is simultaneously occupied by material points X^α of all constituents φ^α (superimposed continua). These particles proceed from different reference positions $\mathbf{X}_\alpha$ at time t_0. Thus, each constituent is assigned an individual motion function

$$\mathbf{x} = \chi_\alpha(\mathbf{X}_\alpha, t). \tag{1}$$

The volume fractions

$$n^\alpha = n^\alpha(\mathbf{x}, t) \tag{2}$$

are defined as the local ratios of the constituent volumes v^α with respect to the bulk volume v. Thus, the saturation conditions yields

$$n^S + n^F = 1. \tag{3}$$

Associated with each constituent φ^α is an effective (realistic or material) density $\rho^{\alpha R}$ and a partial (global or bulk) density ρ^α. The effective density $\rho^{\alpha R}$ is defined as the local mass of φ^α per unit of v^α, whereas the bulk density ρ^α exhibits the same mass per unit of v. The density functions are related by

$$\rho^\alpha = n^\alpha \rho^{\alpha R}. \tag{4}$$

Proceeding from (4), it is obvious that the property of material incompressibility of any constituent φ^α (defined by $\rho^{\alpha R} = \text{const.}$) is not equivalent to global incompressibility of this constituent, since the partial density functions can still change through changes in the volume fractions n^α.

It follows from (1) that each constituent is assigned its own velocity and acceleration fields (Lagrangean description):

$$\overset{\prime}{\mathbf{x}}_\alpha = \frac{\partial \chi_\alpha(\mathbf{X}_\alpha, t)}{\partial t}, \quad \overset{\prime\prime}{\mathbf{x}}_\alpha = \frac{\partial^2 \chi_\alpha(\mathbf{X}_\alpha, t)}{\partial t^2}. \tag{5}$$

With the aid of the inverse motion function χ_α^{-1}, the corresponding Eulerian description reads

$$\overset{\prime}{\mathbf{x}}_\alpha = \overset{\prime}{\mathbf{x}}_\alpha(\mathbf{x}, t), \quad \overset{\prime\prime}{\mathbf{x}}_\alpha = \overset{\prime\prime}{\mathbf{x}}_\alpha(\mathbf{x}, t). \tag{6}$$

Assume that Γ is any arbitrary, continuous and sufficiently often continuously differentiable function of $(\mathbf{x}, t)$. Then, the material time derivatives of Γ corresponding to the individual motion functions of φ^α yield

$$(\Gamma)'_{(\alpha)} = \frac{\partial \Gamma}{\partial t} + \operatorname{grad} \Gamma \cdot \overset{\prime}{\mathbf{x}}_\alpha. \tag{7}$$

Therein, the operator "grad(·)" characterizes the partial derivative of (·) with respect to the position vector $\mathbf{x}$ of the actual configuration.

Concerning the problem of saturated or empty porous skeleton materials, it is convenient to consider the solid motion in the frame of the Lagrangian description by the introduction of the displacement vector

$$\mathbf{u}_S = \mathbf{x} - \mathbf{X}_S, \tag{8}$$

while the pore-fluid is better described by a modified Eulerian formulation, where the seepage velocity $\mathbf{w}_F$ is taken as the kinematic variable characterizing the velocity of the pore-fluid relative to the deforming skeleton:

$$\mathbf{w}_F = \overset{\prime}{\mathbf{x}}_F - \overset{\prime}{\mathbf{x}}_S. \tag{9}$$

From (1) and (8), the material deformation gradient and the displacement gradient of the solid skeleton are:

$$\mathbf{F}_S = \mathrm{Grad}_S\, \mathbf{x}, \quad \mathbf{H}_S = \mathrm{Grad}_S\, \mathbf{u}_S. \tag{10}$$

Therein, the operator "$\mathrm{Grad}_S(\cdot)$" defines the partial derivative of $(\cdot)$ with respect to the reference position $\mathbf{X}_S$ of φ^S. From the displacement gradient, one easily derives the classical measures of the geometrically linearized theory

$$\begin{aligned} \mathbf{H}_{S\,\mathrm{sym}} &= \tfrac{1}{2}(\mathbf{H}_S + \mathbf{H}_S^T) =: \boldsymbol{\varepsilon}_S, \\ \mathbf{H}_{S\,\mathrm{skw}} &= \tfrac{1}{2}(\mathbf{H}_S - \mathbf{H}_S^T) =: \boldsymbol{\varphi}_S \times \mathbf{I}. \end{aligned} \tag{11}$$

Therein, $\boldsymbol{\varepsilon}_S$ is the linear Lagrangean solid strain, $\boldsymbol{\varphi}_S$ is the so-called continuum rotation vector, $\mathbf{I}$ is the second-order identity (fundamental tensor of second order), and $(\cdot)^T$ is the transpose of $(\cdot)$. The external tensor product between vectors and tensors (cf de Boer, 1982) is defined by

$$\boldsymbol{\varphi}_S \times \mathbf{I} = -\overset{3}{\mathbf{E}}\, \boldsymbol{\varphi}_S; \tag{12}$$

$\overset{3}{\mathbf{E}}$ is the Ricci permutation or the fundamental tensor of third-order, respectively. Given $(11)_2$, it is straightforward to obtain $\boldsymbol{\varphi}_S$ as a function of $\mathbf{H}_S$:

$$\boldsymbol{\varphi}_S = -\tfrac{1}{2}\overset{3}{\mathbf{E}}(\mathbf{H}_{S\,\mathrm{skw}}). \tag{13}$$

In extension of the continuum mechanical description of the skeleton material, additional micropolar degrees of freedom are introduced via the independent rotation $\overset{*}{\boldsymbol{\varphi}}_S$, thus, defining the total average grain rotation $\bar{\boldsymbol{\varphi}}_S$, in the framework of the geometrically linearized theory, as the sum of the continuum rotation and the additional micropolar rotation, viz:

$$\bar{\boldsymbol{\varphi}}_S = \boldsymbol{\varphi}_S + \overset{*}{\boldsymbol{\varphi}}_S. \tag{14}$$

By use of the additional micropolar degrees of freedom, the linear Cosserat strain tensor $\boldsymbol{\varepsilon}_{Sc}$ and the linear curvature tensor $\bar{\boldsymbol{\kappa}}_S$ yield:

$$\boldsymbol{\varepsilon}_{Sc} = \mathbf{H}_S + \overset{3}{\mathbf{E}}\, \bar{\boldsymbol{\varphi}}_S, \quad \bar{\boldsymbol{\kappa}}_S = \mathrm{Grad}_S\, \bar{\boldsymbol{\varphi}}_S. \tag{15}$$

The symmetric and skew symmetric parts of the Cosserat strain are

$$\boldsymbol{\varepsilon}_{Sc\,\mathrm{sym}} = \tfrac{1}{2}(\mathbf{H}_S + \mathbf{H}_S^T),$$

$$\boldsymbol{\varepsilon}_{Sc\,\mathrm{skw}} = \tfrac{1}{2}(\mathbf{H}_S - \mathbf{H}_S^T) + \overset{3}{\mathbf{E}}\,\bar{\boldsymbol{\varphi}}_S. \tag{16}$$

In this representation, $\boldsymbol{\varepsilon}_{Sc\,\mathrm{sym}}$ equals the linearized Lagrangian strain $\boldsymbol{\varepsilon}_S$ of non-polar materials, whereas

$$\boldsymbol{\varepsilon}_{Sc\,\mathrm{skw}} = \overset{3}{\mathbf{E}}(\bar{\boldsymbol{\varphi}}_S - \boldsymbol{\varphi}_S) = \overset{3}{\mathbf{E}}\,\overset{*}{\boldsymbol{\varphi}}_S \tag{17}$$

exhibits a tensorial measure for the additional micropolar rotation $\overset{*}{\boldsymbol{\varphi}}_S$. Finally, with the aid of $(16)_1$ and (17), the Cosserat strain $\boldsymbol{\varepsilon}_{Sc}$, alternatively to $(15)_1$, can be expressed by

$$\begin{aligned}\boldsymbol{\varepsilon}_{Sc} &= \tfrac{1}{2}(\mathbf{H}_S + \mathbf{H}_S^T) + \overset{3}{\mathbf{E}}\,\overset{*}{\boldsymbol{\varphi}}_S \\ &= \boldsymbol{\varepsilon}_S + \overset{3}{\mathbf{E}}\,\overset{*}{\boldsymbol{\varphi}}_S.\end{aligned} \tag{18}$$

Furthermore, the Cosserat strain and the linear curvature tensor are related to each other by the micropolar compatibility condition, which can be obtained from $(10)_2$ and (15) by use of the Schwarzian exchangeability rule of partial derivatives:

$$\mathrm{Grad}_S\,\boldsymbol{\varepsilon}_{Sc} - \mathrm{Grad}_S^{\overset{23}{T}}\,\boldsymbol{\varepsilon}_{Sc} = (\overset{3}{\mathbf{E}}\,\bar{\boldsymbol{\kappa}}_S)^{\overset{3}{-}} - (\overset{3}{\mathbf{E}}\,\bar{\boldsymbol{\kappa}}_S)^{\overset{3}{-}\overset{23}{T}}. \tag{19}$$

Therein, the transpositions $(\cdot)^{\overset{ik}{T}}$ indicate an exchange of the i-th and k-th basis systems included into the tensor basis of higher order tensors. The additional topscript $(\cdot)^{\overset{n}{-}}$ defines the included contraction $(\cdot)$ to yield a tensor of n-th order (de Boer, 1982). In a simple index notation, the above compatibility condition has firstly been proposed by Nowacki in 1969 (cf Nowacki, 1986). In general, (19) consists of 27 scalar equations. However, since there are only nine independent equations incorporated into (19), this relation can be solved with respect to $\bar{\boldsymbol{\kappa}}_S$ by use of the methods of the general tensor calculus. Thus,

$$\bar{\boldsymbol{\kappa}}_S = \tfrac{1}{2}\overset{3}{\mathbf{E}}(\mathrm{Grad}_S\,\boldsymbol{\varepsilon}_{Sc} + \mathrm{Grad}_S^{\overset{13}{T}}\,\boldsymbol{\varepsilon}_{Sc} - \mathrm{Grad}_S^{\overset{23}{T}}\,\boldsymbol{\varepsilon}_{Sc})^{\overset{2}{-}}. \tag{20}$$

This representation of the micropolar compatibility condition is a novelty and has firstly been published, as far as the authors are aware, by Ehlers and Volk (1997b). As a result of (20), it follows immediately that once $\boldsymbol{\varepsilon}_{Sc}$ is given, it is straightforward to compute $\bar{\boldsymbol{\kappa}}_S$.

2.2. *Balance relations*

Proceeding from the general geometrically non-linear formulation, the governing balance relations of the problem under consideration can be taken from the relevant literature on the Theory of Porous Media, cf e.g. Bowen (1980), de Boer and Ehlers (1986) or Ehlers (1996). However, under the present circumstances, the balance relations of the standard formulation of the classical TPM must be extended by the introduction of elements of multiphase micropolar theories (cf Diebels and Ehlers, 1996). In the framework of a purely mechanical theory of micropolar multiphase materials, the following balance equations for mass, momentum and moment of momentum (m.o.m.) hold:

- Balance of mass: $(\rho^\alpha)'_\alpha + \rho^\alpha \operatorname{div} \mathbf{x}'_\alpha = \hat{\rho}^\alpha$,
- Balance of momentum: $\rho^\alpha \mathbf{x}''_\alpha = \operatorname{div} \mathbf{T}^\alpha + \rho^\alpha \mathbf{b}^\alpha + \hat{\mathbf{p}}^\alpha$,
- Balance of m.o.m.: $[2\rho^\alpha(\bar{\mathbf{W}}_\alpha \boldsymbol{\Theta}^\alpha)_{\mathrm{sym}} + \hat{\rho}^\alpha \boldsymbol{\Theta}^\alpha]\bar{\boldsymbol{\omega}}_\alpha + \hat{\rho}^\alpha \boldsymbol{\Theta}^\alpha(\bar{\boldsymbol{\omega}}_\alpha)'_\alpha$
  $= \mathbf{I} \times \mathbf{T}^\alpha + \operatorname{div} \mathbf{M}^\alpha + \rho^\alpha \mathbf{c}^\alpha + \hat{\mathbf{m}}^\alpha.$ (21)

In these relations, $\mathbf{T}^\alpha$ is the non-symmetric Cauchy stress tensor of micropolar materials, $\mathbf{b}^\alpha$ is the volume force per unit of φ^α-th mass, $\mathbf{\Theta}^\alpha$ is the tensor of microinertia, $\bar{\boldsymbol{\omega}}_\alpha = (\bar{\boldsymbol{\varphi}}_\alpha)'_\alpha$ is the rotational velocity corresponding to $\bar{\boldsymbol{\varphi}}_\alpha$, $\mathbf{M}^\alpha$ is the couple stress tensor, and $\mathbf{c}^\alpha$ is the body couple stress vector per unit of φ^α-th mass. Furthermore, the quantities $\hat{\rho}^\alpha$, $\hat{\mathbf{p}}^\alpha$ and $\hat{\mathbf{m}}^\alpha$ represent the density production and the direct parts of the momentum production and the moment of momentum production, respectively; "div(·)" is the divergence operator corresponding to "grad(·)".

Furthermore, $\mathbf{I} \times \mathbf{T}^\alpha$ defines twice the axial vector corresponding to the skew-symmetric part of $\mathbf{T}^\alpha$ (de Boer, 1982):

$$\mathbf{I} \times \mathbf{T}^\alpha = -\overset{3}{\mathbf{E}}\, \overset{A}{\mathbf{T}}{}^\alpha = 2\mathbf{t}^\alpha. \tag{22}$$

The quantity

$$\bar{\mathbf{W}}_\alpha = \bar{\boldsymbol{\omega}}_\alpha \times \mathbf{I} \tag{23}$$

denotes the skew-symmetric micropolar gyration tensor (Diebels and Ehlers, 1996) with $\bar{\boldsymbol{\omega}}_\alpha$ as the corresponding axial vector.

The production term included into (21) are restricted to the following constraints:

$$\sum_{\alpha=1}^{k} \hat{\rho}^\alpha = 0,$$

$$\sum_{\alpha=1}^{k} \hat{\mathbf{p}}^\alpha + \hat{\rho}^\alpha \overset{\prime}{\mathbf{x}}_\alpha = \mathbf{0},$$

$$\sum_{\alpha=1}^{k} \hat{\mathbf{m}}^\alpha = \mathbf{0}. \tag{24}$$

Considering the special case of quasi-static processes of a liquid-saturated porous skeleton material and excluding mass exchanges between the solid and the fluid constituents, i.e. $\hat{\rho}^\alpha = 0$, the balance eqns (21) yield:
Balance of mass:

$$0 = (\rho^\alpha)'_\alpha + \rho^\alpha \operatorname{div} \overset{\prime}{\mathbf{x}}_\alpha. \tag{25}$$

Balance of momentum:

$$\mathbf{0} = \operatorname{div} \mathbf{T}^\alpha + \rho^\alpha \mathbf{b} + \hat{\mathbf{p}}^\alpha,$$

$$\hat{\mathbf{p}}^S + \hat{\mathbf{p}}^F = \mathbf{0}. \tag{26}$$

Balance of m.o.m.:

$$\mathbf{0} = \mathbf{I} \times \mathbf{T}^\alpha + \operatorname{div} \mathbf{M}^\alpha + \rho^\alpha \mathbf{c}^\alpha + \hat{\mathbf{m}}^\alpha,$$

$$\hat{\mathbf{m}}^S + \hat{\mathbf{m}}^F = \mathbf{0}. \tag{27}$$

In $(26)_1$, it has been assumed that $\mathbf{b}^\alpha$ is the gravity force. Thus, $\mathbf{b}^\alpha = \mathbf{b} \forall \varphi^\alpha$. Furthermore, to obtain the above representation of $(27)_1$, the well-known simplifying assumption of spherical microparticles has been applied to yield $(\bar{\mathbf{W}}_\alpha \mathbf{\Theta}^\alpha)_{\text{sym}} = \mathbf{0}$.

Moreover, the consideration of a binary model consisting of a micropolar skeleton and a non-polar pore-fluid where $\hat{\mathbf{m}}^F = \mathbf{0}$ (de Boer *et al.*, 1991), substitutes (27) by

$$\mathbf{0} = \mathbf{I} \times \mathbf{T}^S + \operatorname{div} \mathbf{M}^S + \rho^S \mathbf{c}^S,$$

$$\mathbf{T}^F = (\mathbf{T}^F)^T. \tag{28}$$

Based on the property of material incompressibility of both constituents ($\rho^{\alpha R} = \text{const.}$), solid skeleton and pore-liquid, the sum of the individual mass balance eqns (25), the saturation condition (3) and the density relation (4) combine to yield:

$$\operatorname{div}[n^F \mathbf{w}_F + (\mathbf{u}_S)'_S] = 0. \tag{29}$$

This equation represents the volume balance relation or the incompressibility constraint of the binary material under study:

3. CONSTITUTIVE MODELLING

3.1. *General setting*

In order to close the set of governing equations for the liquid-saturated micropolar skeleton material under study, constitutive equations must be formulated for the solid and the fluid stress tensors $\mathbf{T}^\alpha (\alpha \in \{S, F\})$, the solid couple stress tensor $\mathbf{M}^S$ and for the interaction force (direct momentum production) $\hat{\mathbf{p}}^F = -\hat{\mathbf{p}}^S$. As a result of the incompressibility assumption of both materials, the expressions for the stress tensors and for the interaction force consist of two terms each:

$$\mathbf{T}^\alpha = -n^\alpha p \mathbf{I} + \mathbf{T}^\alpha_E,$$

$$\hat{\mathbf{p}}^F = p \operatorname{grad} n^F + \hat{\mathbf{p}}^F_E. \tag{30}$$

The first term in these relations includes the Lagrangian multiplier p, which can be identified as the effective liquid pressure, while the second term, in the sense of an extra quantity, index $(\cdot)_E$, is governed by the solid deformation and the pore-liquid viscosity (Ehlers, 1989). In solid mechanics, the solid extra stress is known, following Terzaghi (1923), as the effective stress of the soil material (de Boer and Ehlers, 1990). As is usual in hydraulics, it is assumed that the liquid extra stress or the frictional stress, respectively, can be neglected in comparison to the other terms incorporated into the momentum balance relation of φ^F. Thus, the *a priori* assumption $\mathbf{T}^F_E = \mathbf{0}$ is applied. The internal friction between the skeleton and the viscous pore-liquid is taken into account by the effective drag force or the direct momentum production term, viz:

$$\hat{\mathbf{p}}^F_E = -\frac{(n^F)^2 \gamma^{FR}}{k^F} \mathbf{w}_F. \tag{31}$$

Therein, $\gamma^{FR} = \rho^{FR}|\mathbf{b}|$ is the effective (true) specific weight of the pore-liquid and k^F is the Darcy permeability coefficient, which is generally given as a function of the porosity or the solid deformation, respectively. In the framework of geometrically linear theories, it is assumed that

$$k^F = k^F_0 [1 + m^k n^S_{0S} (\boldsymbol{\varepsilon}_{Sc} \cdot \mathbf{I})]. \tag{32}$$

In this relation, m^k is a material number, and n^S_{0S} is the solid volume fraction in the reference configuration of φ^S. Furthermore, k^F is related to the intrinsic (or physical) permeability parameter K^S of the skeleton material via

$$k^F = \frac{\gamma^{FR}}{\mu^{FR}} K^S; \tag{33}$$

μ^{FR} is the effective shear viscosity parameter of φ^F. It follows from (33) that the permeability parameter k^F, in the sense of a macroscopic quantity, provides information about both the local size and isotropic structure of the pore-space and the fluid viscosity.

3.2. *Polar and non-polar elasto-plastic frictional skeleton materials*

The following considerations are based on the assumptions of geometrically linear deformations, where the elasto-plastic Cosserat strain $\boldsymbol{\varepsilon}_{Sc}$ is additively decomposed into elastic and plastic parts. Thus, from this decomposition and the micropolar compatibility condition (20), it is straightforward to conclude that the elasto-plastic curvature tensor $\bar{\boldsymbol{\kappa}}_S$ must also be additively decomposed into elastic and plastic parts, viz:

$$\begin{aligned} \boldsymbol{\varepsilon}_{Sc} &= \boldsymbol{\varepsilon}_{Sce} + \boldsymbol{\varepsilon}_{Scp}, \\ \bar{\boldsymbol{\kappa}}_S &= \bar{\boldsymbol{\kappa}}_{Se} + \bar{\boldsymbol{\kappa}}_{Sp}. \end{aligned} \tag{34}$$

In extension of the Hookean elasticity model, the constitutive equation of the non-symmetric solid extra stress reads

$$\mathbf{T}_E^S = [2\mu^S \overset{4}{\mathbf{I}}_{\text{sym}} + 2\mu_c^S \overset{4}{\mathbf{I}}_{\text{skw}} + \lambda^S (\mathbf{I} \otimes \mathbf{I})]\boldsymbol{\varepsilon}_{Sce}, \tag{35}$$

where

$$\begin{aligned} \overset{4}{\mathbf{I}}_{\text{sym}} &= \tfrac{1}{2}[(\mathbf{I} \otimes \mathbf{I})^{\overset{23}{T}} + (\mathbf{I} \otimes \mathbf{I})^{\overset{13}{T}}], \\ \overset{4}{\mathbf{I}}_{\text{skw}} &= \tfrac{1}{2}[(\mathbf{I} \otimes \mathbf{I})^{\overset{23}{T}} - (\mathbf{I} \otimes \mathbf{I})^{\overset{13}{T}}]. \end{aligned} \tag{36}$$

The application of the fundamental tensors of fourth order, $\overset{4}{\mathbf{I}}_{\text{sym}}$ and $\overset{4}{\mathbf{I}}_{\text{skw}}$, to an arbitrary second order tensor yields its symmetric and its skew-symmetric parts. The material parameters μ^S and λ^S are the Lamé constants of the porous skeleton material, whereas μ_c^S is an additional parameter governing the influence of the skew-symmetric part of the elastic Cosserat strain $\boldsymbol{\varepsilon}_{Sce}$ on the effective stress of the skeleton material. In analogy to the strain relation (18), the symmetric part of $\mathbf{T}_E^S$ represents the solid stress for non-polar skeleton materials, whereas the skew-symmetric part of polar skeleton materials is directly related to the independent micropolar rotation $\overset{*}{\boldsymbol{\varphi}}_S$. Finally, it should be noted that in case of materially incompressible skeletons, λ^S includes the structural compression modulus (Ehlers, 1993a, b), thus governing the influence of elastic volume strains based on local porosity variations on the macroscopic stress behaviour.

Concerning the constitutive equation governing the couple stress tensor, the general assumption must be chosen in analogy to (35). Thus,

$$\mathbf{M}^S = [2\bar{\mu}^S \overset{4}{\mathbf{I}}_{\text{sym}} + 2\bar{\mu}_c^S \overset{4}{\mathbf{I}}_{\text{skw}} + \bar{\lambda}^S (\mathbf{I} \otimes \mathbf{I})]\bar{\boldsymbol{\kappa}}_{Se}. \tag{37}$$

Basically, $\bar{\mu}^S$, $\bar{\mu}_c^S$ and $\bar{\lambda}^S$ in (37) have the same meaning as μ^S, μ_c^S and λ^S in (35), however, $\bar{\mu}^S$, $\bar{\mu}_c^S$ and $\bar{\lambda}^S$ do not relate the elastic Cosserat strain tensor to the non-symmetric stress tensor but the elastic curvature tensor to the couple stress tensor. However, because there is a considerable uncertainty concerning the experimental determination of the material parameters included into (37), it is convenient with respect to the numerical computations to apply the simplified set-up by de Borst (1991) instead of (37):

$$\mathbf{M}^S = 2\mu^S (l_c^S)^2 \bar{\boldsymbol{\kappa}}_{Se}. \tag{38}$$

Proceeding from (38), the assumption $\bar{\mu}^S = \bar{\mu}_c^S = \mu^S (l_c^S)^2$ is made, where l_c^S is usually interpreted as an internal length scale parameter. Thus, l_c^S implicitly offers the possibility to include the shear band width into the model; however, l_c^S cannot be taken as the shear band width itself.

In order to describe the plastic material properties of both non-polar and polar skeleton materials, one has to introduce a convenient yield function to bound the elastic domain together with evolution equations for the non-symmetric plastic strain rate $(\boldsymbol{\varepsilon}_{Scp})'_S$ and the plastic rate of curvature tensor $(\bar{\boldsymbol{\kappa}}_{Sp})'_S$. Throughout the present article, use is made of the ideal plasticity concept.

Concerning the introduction of a yield function for frictional porous materials, an extension of the single-surface yield criterion by Ehlers (1993a, 1995) is applied, compare Fig. 1. By extension of the original yield function towards the most general case of micro-polar cohesive–frictional materials, one obtains

$$\begin{aligned} F^c &= \Phi^{1/2} + \beta \mathrm{I} + \varepsilon \mathrm{I}^2 - \kappa = 0, \\ \Phi &= \mathrm{II}_{D\,\mathrm{sym}} (1 + \gamma \vartheta)^m + \tfrac{1}{2}\alpha \mathrm{I}^2 + \delta^2 \mathrm{I}^4 + k_1 \mathbf{M}^S \cdot \mathbf{M}^S + k_2 \mathrm{II}_{\mathrm{skw}}, \\ \vartheta &= \mathrm{III}_{D\,\mathrm{sym}} / (\mathrm{II}_{D\,\mathrm{sym}})^{3/2}. \end{aligned} \tag{39}$$

In this representation $\mathscr{P} = \{\alpha, \beta, \gamma, \delta, \varepsilon, m, \kappa, k_1, k_2\}$ is a set of nine material parameters; I, $\mathrm{II}_{D\,\mathrm{sym}}$ and $\mathrm{III}_{D\,\mathrm{sym}}$ are the first and deviatoric (negative) second and third principal invariants of the symmetric part of the effective stress $\mathbf{T}_E^S$, whereas $\mathrm{II}_{\mathrm{skw}}$ defines the second principal invariant of the skew-symmetric part of $\mathbf{T}_E^S$:

$$\begin{aligned} \mathrm{I} &= \mathbf{T}_E^S \cdot \mathbf{I}, \\ \mathrm{II}_{D\,\mathrm{sym}} &= \tfrac{1}{2} \mathbf{T}_{E\,\mathrm{sym}}^{SD} \cdot \mathbf{T}_{E\,\mathrm{sym}}^{SD}, \\ \mathrm{II}_{\mathrm{skw}} &= \tfrac{1}{2} \mathbf{T}_{E\,\mathrm{skw}}^{S} \cdot \mathbf{T}_{E\,\mathrm{skw}}^{S}, \\ \mathrm{III}_{D\,\mathrm{sym}} &= \tfrac{1}{3} \mathbf{T}_{E\,\mathrm{sym}}^{SD} \cdot (\mathbf{T}_{E\,\mathrm{sym}}^{SD} \mathbf{T}_{E\,\mathrm{sym}}^{SD}). \end{aligned} \tag{40}$$

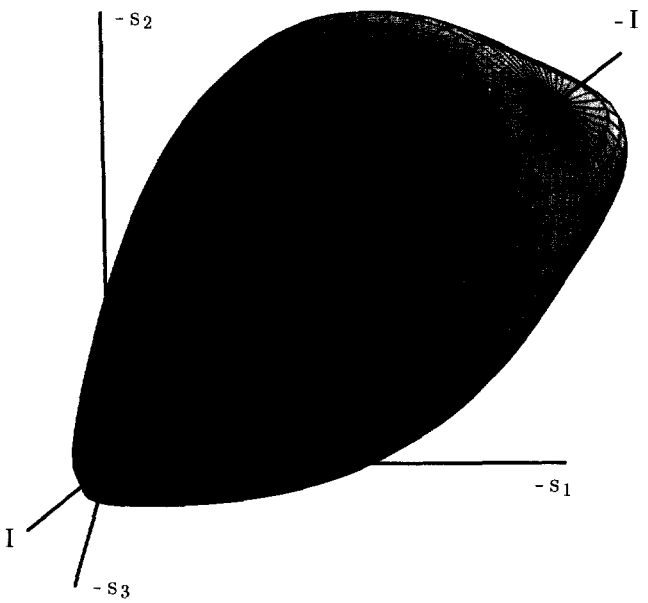

Fig. 1. Single-surface yield criterion for non-polar cohesive–frictional materials; s_1, s_2, s_3: principal stresses $\mathbf{T}_{E\,\mathrm{sym}}^S$ (tension positive).

The index $(\cdot)^D$ characterizes the deviatoric part of the respective tensorial object. The material parameters α, β, δ, ε and κ govern the representation of the yield surface in the hydrostatic plane, whereas the parameters γ and m are responsible for the smoothly triangular yield curve in the deviatoric plane. For an extended discussion of the single-surface criterion (39) and its application to non-polar cohesive-frictional materials, the reader is referred to Ehlers (1995). In addition to the first seven material parameters included in the set $\mathscr{P}$, k_1 and k_2 additionally introduce the skeleton's micropolarity properties into the yield criterion, thus governing the influence of the couple stress and the skew-symmetric part of the effective skeleton stress on the onset of plastic yielding. Note in passing that (39) is different from the suggestion made by Ehlers and Volk (1997a). In particular, the influence of micropolarity has been included into the function Φ in order to additionally govern the deviatoric shape of F^c. In the framework of dilatant frictional materials, softening effects occurring in the localization zones can be described even in the framework of the ideal plasticity concept. Furthermore, the ideal plasticity concept implies that all material parameters of the yield criterion are constants, where the following relations between β and κ and the angle of internal friction ϕ and the cohesion c hold:

$$\beta = \tfrac{1}{3}\sin\phi, \quad \kappa = c\cos\phi. \tag{41}$$

The reader who is interested in further information on the adjustment of the included material parameters to test results, is referred to Ehlers (1993a, 1995). However, concerning the determination of k_1 and k_2, further experimental data is necessary, which has not been produced by laboratory tests yet.

In addition to the single-surface yield function defined above, evolution equations (flow rules) for the plastic Cosserat strain rate $(\varepsilon_{Scp})'_S$ and the plastic rate of curvature tensor $(\bar{\kappa}_{Sp})'_S$ must be considered. Concerning the representation of these equations, one has to take into account that the usual associated flow rule concept cannot be applied to frictional materials (cf e.g. Lade and Duncan, 1973). In particular, the use of an associated flow rule for $(\varepsilon_{Scp})'_S$ would predict completely wrong results in the description of the deviatoric part and, even worse, of the volumetric part of the plastic strain rate (dilatancy and contractancy). Thus, in the framework of the non-associated plasticity, an additional plastic potential function is introduced, viz:

$$\begin{aligned} G^c &= \Gamma^{1/2} + \beta \mathrm{I} + \varepsilon \mathrm{I}^2 - g(\mathrm{I}) = 0, \\ \Gamma &= \mathrm{II}_{D\,\mathrm{sym}} + \tfrac{1}{2}\alpha \mathrm{I}^2 + \delta^2 \mathrm{I}^4 + k_2 \mathrm{II}_{\mathrm{skw}}. \end{aligned} \tag{42}$$

The difference between the yield function (39) and the plastic potential function (42) results in the fact that (42) exhibits, in the principal stress space of non-polar materials, a circular shape in the deviatoric plane, whereas (39) is characterized by a triangular shape with rounded corners. The function $g(\mathrm{I})$ serves to adjust of the dilatation angle ν_p to test results, compare Figs 2 and 3.

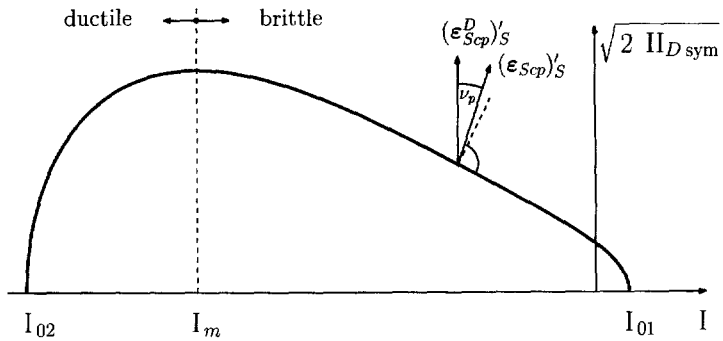

Fig. 2. Hydrostatic plane of the single-surface yield criterion for cohesive–frictional materials.

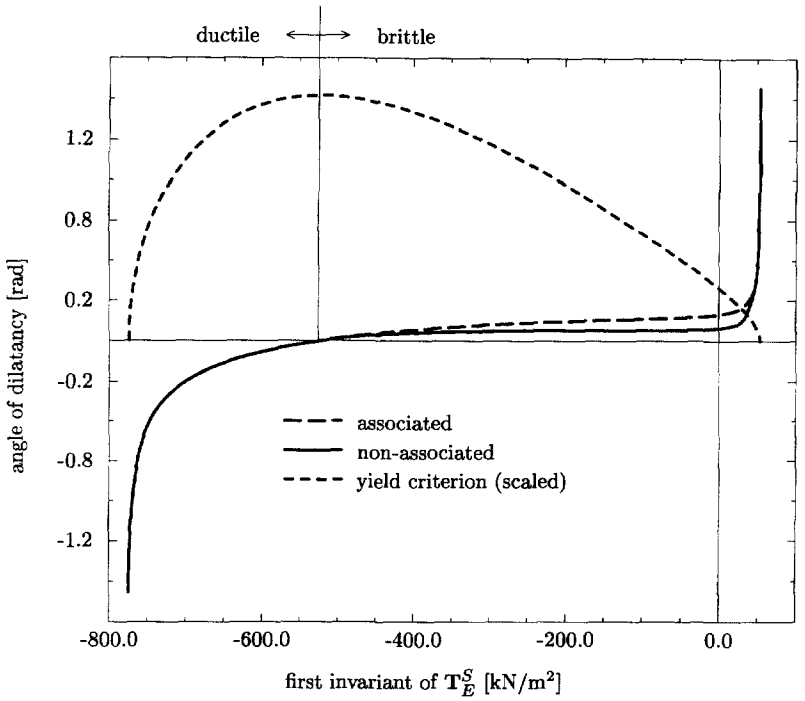

Fig. 3. Dilatation angle of the non-associated flow rule.

Once the plastic potential is given, it is straightforward to determine the plastic strain rate by differentiation of G^c with respect to the effective solid stress:

$$(\boldsymbol{\varepsilon}_{Scp})'_S = \Lambda \frac{\partial G^c}{\partial \mathbf{T}_E^S}. \tag{43}$$

In good accordance with experimental data, this relation predicts co-axial behaviour of the deviatoric part of $(\boldsymbol{\varepsilon}_{Scp})'_S$. Concerning the volumetric part, the function $g(\mathrm{I})$ is chosen in such a way that the direction of $(\boldsymbol{\varepsilon}_{Scp})'_S$, in the brittle range, approximately lies in the middle between the associated and the deviatoric direction, compare Fig. 3. In the ductile range and at the tip of the yield surface, $g(\mathrm{I})$ predicts associated behaviour. Note in passing that, in the framework of the non-associated plasticity concept, the introduction of an additional plastic potential function instead of the direct assumption of a non-associated flow rule (as was proposed by Ehlers and Volk, 1997a) yields considerable numerical advantages.

In the literature on micropolar elasto-plasticity, it is usually assumed that the flow rule for $(\boldsymbol{\kappa}_{Sp})'_S$ is independent from the flow rule for $(\boldsymbol{\varepsilon}_{Scp})'_S$. Consequently, an additional evolution equation is proposed. This procedure has also been applied by the authors (Ehlers and Volk, 1997a). However, it was found that one obtains a very inconvenient convergence behaviour in the framework of finite element computations, when the micropolar degrees of freedom are active, e.g. in the location zone. This bad convergence immediately vanishes, when the micropolar compatibility condition is used, i.e. when the independent flow rule for $(\bar{\boldsymbol{\kappa}}_{Sp})'_S$ is substituted by an evolution equation directly related from (20) and (43) (Ehlers and Volk, 1997b). Thus,

$$(\bar{\boldsymbol{\kappa}}_{Sp})'_S = \tfrac{1}{2}\overset{3}{\mathbf{E}}(\mathrm{Grad}_S(\boldsymbol{\varepsilon}_{Scp})'_S + \mathrm{Grad}_S^{\overset{13}{T}}(\boldsymbol{\varepsilon}_{Scp})'_S - \mathrm{Grad}_S^{\overset{23}{T}}(\boldsymbol{\varepsilon}_{Scp})'_S)^{\overset{2}{-}}. \tag{44}$$

4. WEAK FORMULATION OF THE GOVERNING FIELD EQUATIONS

Based on consideration of four independent fields, the solid displacement $\mathbf{u}_S$, the seepage velocity $\mathbf{w}_F$, the effective liquid pressure p (pore pressure) and the total average

grain rotation $\bar{\boldsymbol{\varphi}}_S$, the corresponding four equations of the weak formulation can be obtained from the kinematics, the balance relations and the constitutive equations of the model under study. Concerning the quasi-static problem under consideration, the seepage velocity can be eliminated by use of the momentum balance of the pore-fluid. Thus, $\mathbf{w}_F$ loses the status of an independent field variable, and the number of equations of the weak formulation reduces to three. These equations are given by the solid and fluid momentum balance eqns $(26)_1$, the volume balance relation (29) and the moment of momentum balance eqn $(28)_1$ of the solid material.

The first equation results from the sum of the solid and the fluid momentum balance equations multiplied by the test function $\delta\mathbf{u}_S$, viz:

$$\int_{\mathscr{V}} (\mathbf{T}_E^S - p\mathbf{I}) \cdot \operatorname{grad} \delta\mathbf{u}_S \, \mathrm{d}v - \int_{\mathscr{V}} (n^F \rho^{FR} + n^S \rho^{SR}) \mathbf{b} \cdot \delta\mathbf{u}_S \, \mathrm{d}v = \int_{\mathscr{S}} \mathbf{t} \cdot \delta\mathbf{u}_S \, \mathrm{d}a. \tag{45}$$

Therein, $\mathbf{t}$ is the external load vector acting upon both constituents. Concerning the pore-liquid, one obtains from the momentum balance $(26)_1$ together with the constitutive eqns (30) and (31) and the density relation (4) that

$$n^F \mathbf{w}_F = -\frac{k^F}{\gamma^{FR}} (\operatorname{grad} p - \rho^{FR} \mathbf{b}). \tag{46}$$

The second equation

$$\int_{\mathscr{V}} \operatorname{div} [n^F \mathbf{w}_F + (\mathbf{u}_S)'_S] \delta p \, \mathrm{d}v = 0 \tag{47}$$

represents the incompressibility constraint of both materials given by the volume balance (29) of the whole aggregate multiplied by the test function δp. Insertion of (46) into (47) yields

$$\int_{\mathscr{V}} \operatorname{div}(\mathbf{u}_S)'_S \delta p \, \mathrm{d}v + \int_{\mathscr{V}} \frac{k^F}{\gamma^{FR}} (\operatorname{grad} p - \rho^{FR} \mathbf{b}) \cdot \operatorname{grad} \delta p \, \mathrm{d}v = -\int_{\mathscr{S}} n^F \mathbf{w}_F \cdot \mathbf{n} \delta p \, \mathrm{d}a, \tag{48}$$

where $\mathbf{n}$ is the outward oriented unit surface normal. In order to complete the set of equations, multiplication of the moment of momentum balance $(28)_1$ by the test function $\delta\bar{\boldsymbol{\varphi}}_S$ results in

$$\int_{\mathscr{V}} (\mathbf{I} \times \mathbf{T}^S + \operatorname{div} \mathbf{M}^S + \rho^S \mathbf{c}^S) \cdot \delta\bar{\boldsymbol{\varphi}}_S \, \mathrm{d}v = 0. \tag{49}$$

Proceeding from the assumption that there is no external loading by couple stress vectors $\mathbf{c}^S$ and surface couples $\mathbf{m}^S = \mathbf{M}^S\mathbf{n}$, one obtains instead of (49):

$$\int_{\mathscr{V}} (\mathbf{I} \times \mathbf{T}^S) \cdot \delta\bar{\boldsymbol{\varphi}}_S \, \mathrm{d}v - \int_{\mathscr{V}} \mathbf{M}^S \cdot \operatorname{Grad}_S \delta\bar{\boldsymbol{\varphi}}_S \, \mathrm{d}v = 0. \tag{50}$$

The eqns (45), (48) and (50) represent the so-called displacement–rotation–pressure formulation of the problem, which has basically been used throughout the following numerical examples. In case of non-polar skeleton materials, these equations reduce to the well-known displacement–pressure formulation, where (50) is dropped. Furthermore, the empty skeleton material is either computed from (45) and (50) or from (45) alone with $p \equiv 0$ and $n^F \equiv 0$. Finally, in the framework of the standard Galerkin procedure, the

included test function $\delta\mathbf{u}_S$, δp and $\delta\bar{\boldsymbol{\varphi}}_S$ and the related weighting functions coincide and correspond to respective field quantities.

Concerning the quasi-static model under consideration, a spatial discretization of the governing weak equations yields with the aid of finite element discretization techniques a matrix differential equation of first order in time:

$$\boldsymbol{M}\frac{\mathrm{d}\boldsymbol{u}}{\mathrm{d}t}+\boldsymbol{k}(\boldsymbol{u})=\boldsymbol{f}. \tag{51}$$

Therein, $\boldsymbol{M}$ is the generalized mass matrix, $\boldsymbol{k}(\boldsymbol{u})$ is the global stiffness vector, $\boldsymbol{u}$ is the vector of the unknown field functions, and $\boldsymbol{f}$ is the generalized force vector. As a consequence of the material incompressibility constraint of both constituents, solid skeleton and pore-fluid, there is no evolution equation for the effective liquid pressure p. Thus, one obtains a system of differential-algebraic equations (DAE) in time, i.e. $\boldsymbol{M}$ included into (51) does not have the full rank.

The final step toward a finite element discretization is to choose the element types and the associated shape functions. Proceeding from triangular elements with six nodes, the unknown fields are approximated either by linear or by quadratic shape functions. In particular, quadratic shape functions have been used to approximate $\mathbf{u}_S$, whereas linear shape functions have been applied for p and $\bar{\boldsymbol{\varphi}}_S$.

5. NUMERICAL EXAMPLES

Concerning the following numerical examples, the included material parameters are fitted in comparison with Schad's model (Schad, 1979), compare Table 1.

Example 1 : *Slope failure induced by an excavation process*

The first numerical example describes the geotechnical slope failure problem induced by an excavation process, compare Fig. 4.

From the classical literature (cf e.g. Terzaghi and Jelinek, 1954), it is well known that the onset of the failure process depends on the actual excavation height and on the angle of the excavated slope. Once a critical height is reached, the upper part of the slope (dark shaded region) is sliding down along the failure line under an angle of $45^\circ-\phi/2$; ϕ is the angle of internal friction of the soil material. Concerning the present example, ϕ can be

Table 1. Material parameters

Parameter	Symbol	Value
Lamé constants	μ^S	5583 kN/m^2
	λ^S	8375 kN/m^2
Effective densities	ρ^{SR}	2600 kg/m^3
	ρ^{FR}	1000 kg/m^3
Volume fractions	n^S_{0S}	0.67
	n^F_{0S}	0.33
Effective liquid weight	γ^{FR}	10 kN/m^3
Permeability	k^F_0	$1.2\cdot10^{-7}$ m/s
	m^k	100
Parameters of the single-surface yield criterion	α	$1.0740\cdot10^{-2}$
	β	0.1195
	γ	1.555
	δ	$1.377\cdot10^{-4}$ m^2/kN
	ε	$4.330\cdot10^{-6}$ m^2/kN
	κ	10.27 kN/m^2
	m	0.5935
Cosserat parameters	l^S_c	$1\cdot10^{-3}$ m
	μ^S_c	$5\cdot10^3$ kN/m^2
	k_1	0
	k_2	1

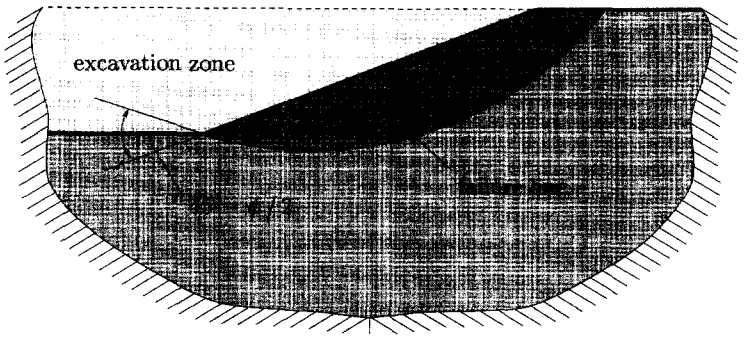

Fig. 4. Slope failure induced by an excavation process.

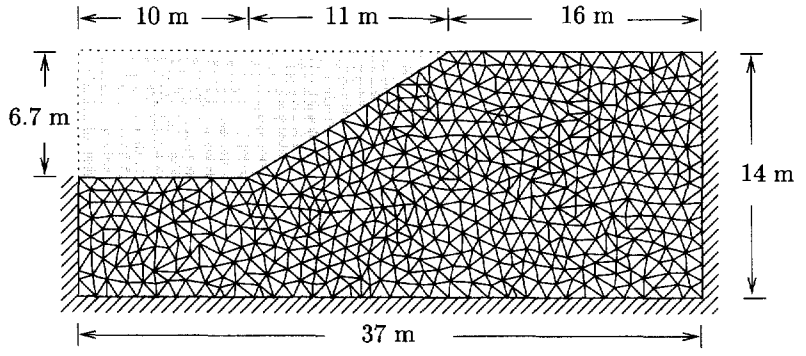

Fig. 5. Geometry and initial mesh of the FE computations.

obtained from (41) with β from Table 1 to yield 21°. Around the failure line, a shear band occurs, namely as a result of a localization of plastic deformations.

In the numerical simulation, an excavation velocity of 0.67 m/day was assumed; the critical height was found at 6.70 m. The geometry and the initial mesh of the finite element computations can be taken from Fig. 5. However, a remeshing strategy is applied, when plastic deformations occur. The following figures show the results of the numerical computations. Three different combinations of material properties have been used to solve the problem. In particular, an empty micropolar solid skeleton (Fig. 6), a liquid-saturated

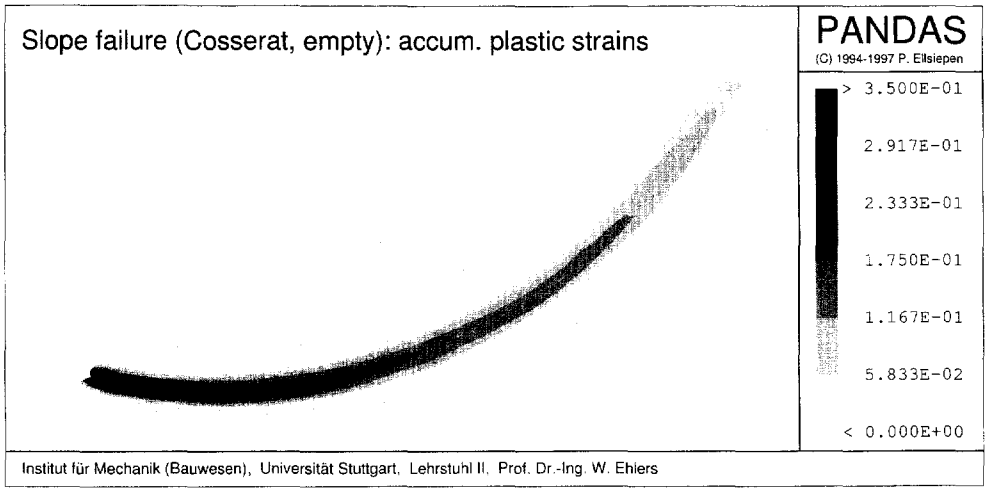

Fig. 6. Empty micropolar skeleton immediately after having reached the critical height.

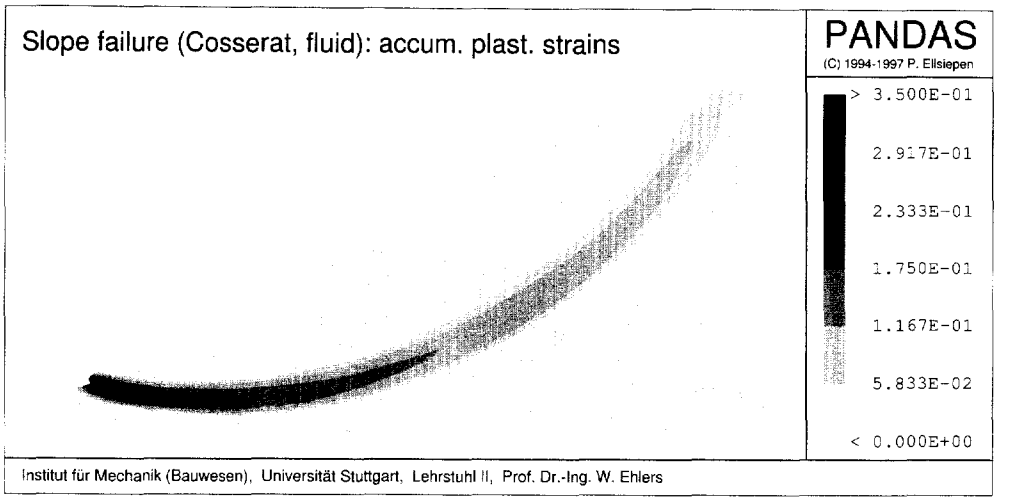

Fig. 7. Saturated micropolar skeleton 20 days after having reached the critical height.

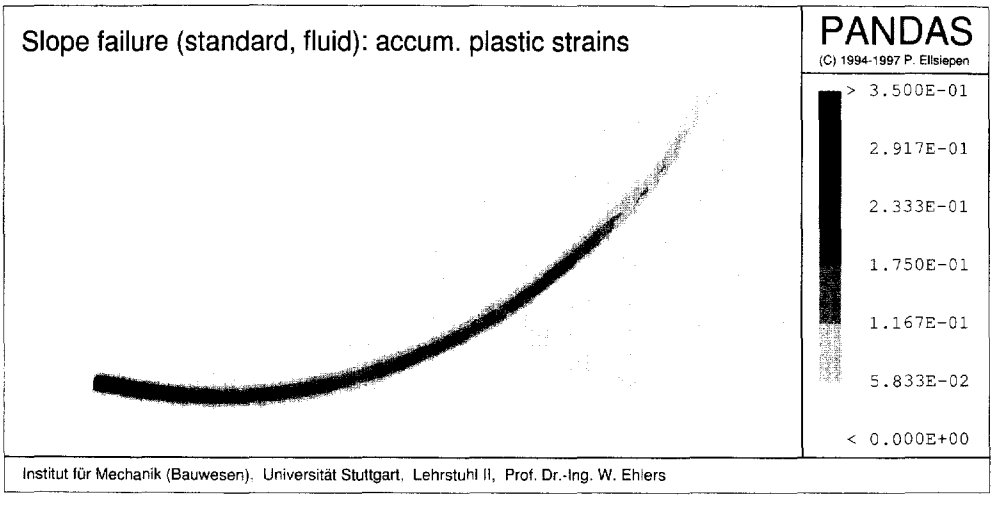

Fig. 8. Saturated non-polar skeleton 20 days after having reached the critical height.

micropolar solid skeleton (Fig. 7) and a liquid-saturated non-polar solid skeleton (Fig. 8) have been investigated. In any case, the onset of the failure process occurred when the critical height was reached. Concerning the empty skeleton (Fig. 6), the complete failure process proceeds instantaneously after having reached the critical height. Also in case of the liquid-saturated skeleton, the failure process immediately starts when the critical height is reached. On the other hand, as a result of the included fluid viscosity, no instantaneous course of the complete process can be observed. Instead, a time-dependent process takes place, which lasts several days in case of the present examples. Figures 7 and 8 show the failure states 20 days after having reached the critical height. The development of the shear bands is easily observed; however, in the saturated case, these bands exhibit a slightly weaker development than the bands in the unsaturated case.

As a result of these and further investigations, the following conclusions can be made:

(a) The localization problem of an empty non-polar skeleton cannot be realized numerically (ill-posed problem).
(b) The inclusion of micropolar degrees of freedom and the inclusion of fluid viscosity both yield a regularization of the numerical shear band problem.

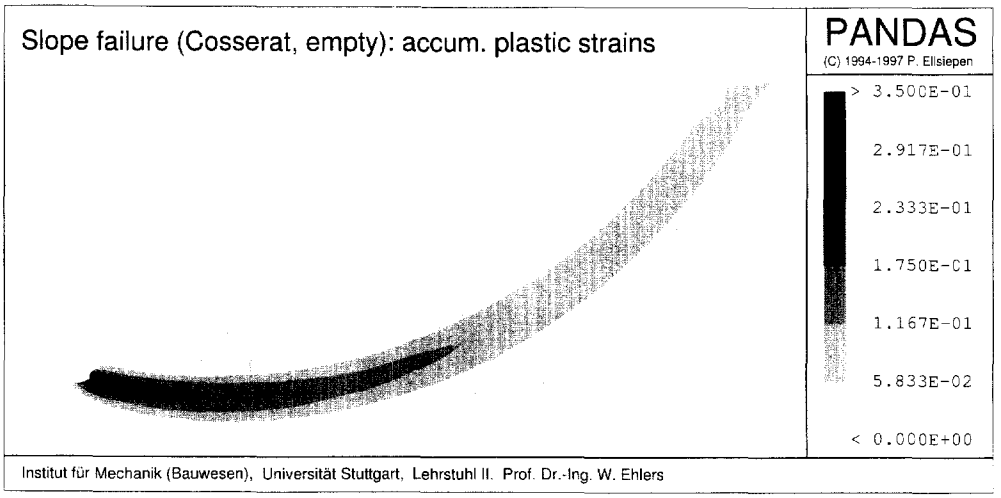

Fig. 9. Empty micropolar skeleton with $l_c^S = 50$ mm.

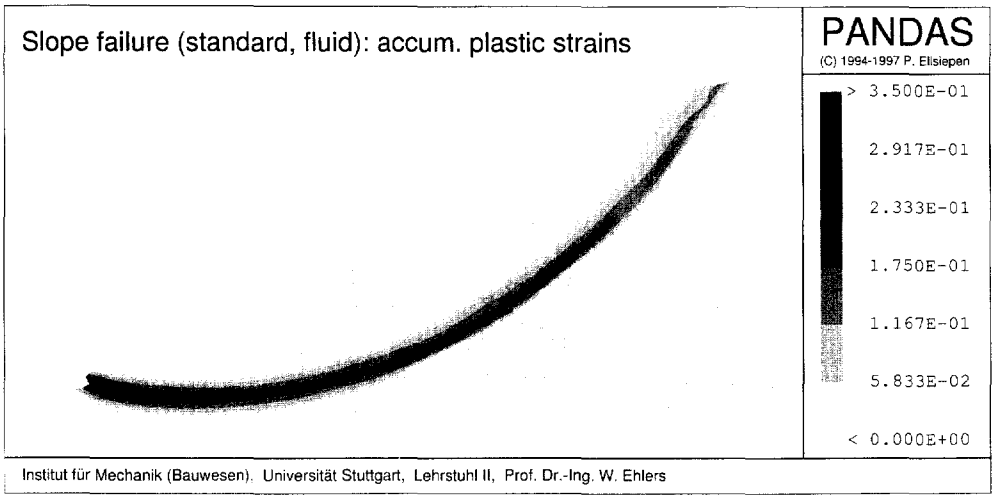

Fig. 10. Saturated non-polar skeleton with $k_0^F = 1.2 \cdot 10^{-10}$ m/s.

(c) The shear band width implicitly depends on the internal length scale parameter l_c as well as on the viscosity of the included fluid.

Concerning the last remark, consider Figs 9 and 10 in comparison with Figs 6 and 8, where the influence of both the internal length scale and the fluid viscosity on the shear band width is demonstrated. In particular, describing an empty micropolar material, it is seen from Figs 6 and 9 that an increase of l_c^S from 1 mm (cf Table 1) to 50 mm yields a significant increase of the shear band width. To show the influence of the Darcy permeability parameter on the shear band width, compare Figs 8 and 10. With respect to the saturated non-polar material, these figures show that a decrease of k_0^F from $1.2 \cdot 10^{-7}$ m/s (cf Table 1) to $1.2 \cdot 10^{-10}$ m/s also leads to an increase of the shear band width. However, since modifications of k_0^F either imply variations of the intrinsic permeability K^S or of the included effective fluid shear viscosity μ^{FR}, cf (33), it is easily concluded that a variation k_0^F means a modification of the basic material properties. In contrast to this, a modification of the length scale parameter included into micropolar theories only influences the shear band width itself, since the additional micropolar degrees of freedom are only active in the

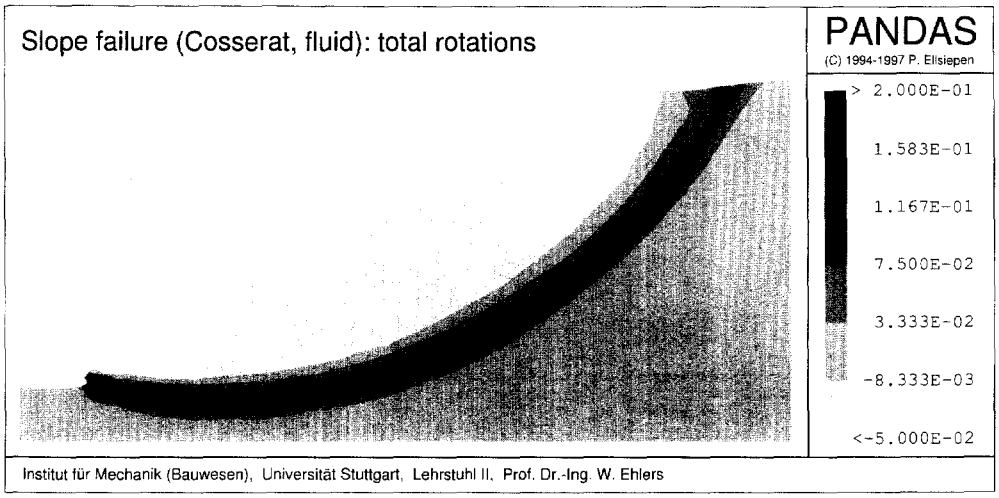

Fig. 11. Total average grain rotation of the saturated micropolar skeleton 20 days after having reached the critical height.

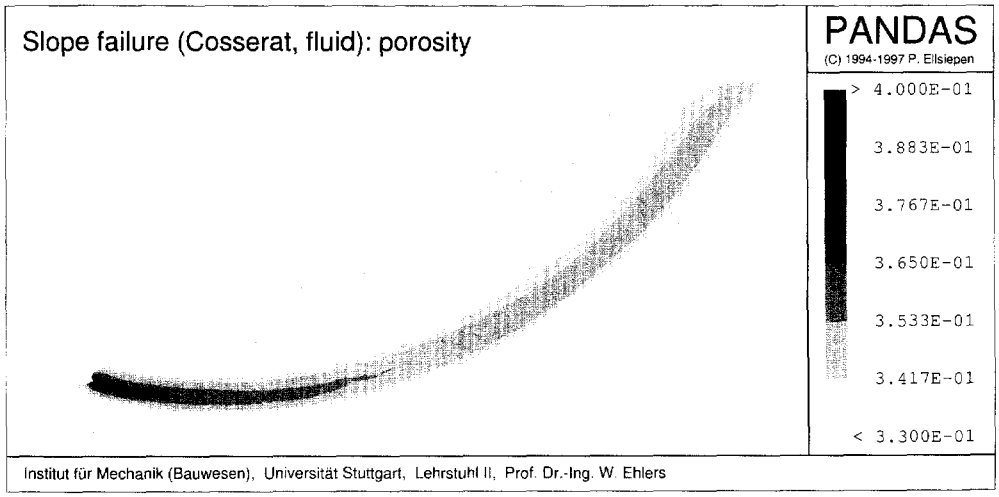

Fig. 12. Porosity localization of the saturated micropolar skeleton 20 days after having reached the critical height.

localization zones, cf Fig. 11. Finally, Figs 6–11 furthermore show that micropolarity is a much stronger regularization tool than fluid viscosity.

In Fig. 11, the influence of the total average grain rotations is plotted. It is easily seen that the rotations occur in the failure zone, where the individual grains of granular materials are rolling one upon the other. Figure 12 exhibits the localization of the porosity variable n^F. It is seen from this figure that a porosity localization (dilatation) occurs in the same area as the localization of the accumulated plastic strains. Finally, Fig. 13 shows the extra pore pressure distribution defined as the local pore pressure minus the pore pressure distribution related to the gravity force of a comparable purely elastic computation. In particular, it is seen from the negative extra pore pressure distribution (extra pore suction) that the fluid tends to flow into the dilatation area. Of course, at the outer surface boundary, a zero pore pressure distribution was prescribed.

Example 2: *Biaxial test*

Based on the material parameters of Table 1, the second example concerns a numerical simulation of a biaxial test of an empty porous solid material, compare Fig. 14. This

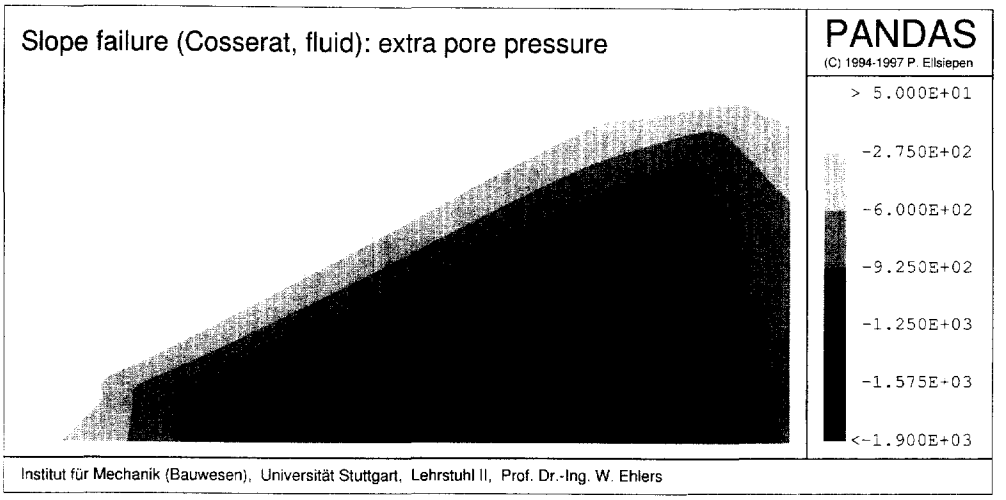

Fig. 13. Extra pore pressure distribution of the saturated micropolar skeleton 20 days after having reached the critical height.

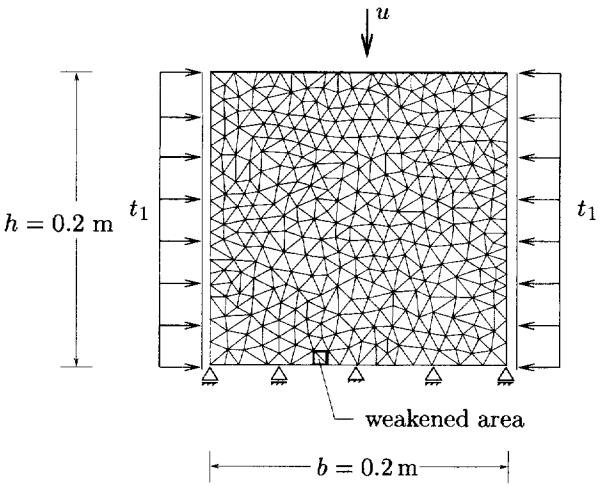

Fig. 14. Course mesh for the numerical biaxial test.

problem is characterized by a constant horizontal load of $t_1 = 100$ kN/m^2 and a time-depending surface displacement of $u = 0.2t \cdot$ mm/s. To stimulate a localization process, the generally homogeneous problem is subjected to a local decrease of the Lamé constants μ^S and λ^S by 1% in the weakened area. The computations have been carried out on a course mesh (651 elements), a medium mesh (1284 elements) and a fine mesh (1856 elements).

The load–displacement curves computed on the three different meshes are plotted in Fig. 15. The left representation exhibits the results obtained by use of the standard formulation (non-polar skeleton). It is easily seen that the load displacement curve, even for the source mesh computations, tends to yield a vertical tangent. Concerning the computations on the middle mesh and the fine mesh, no results can be obtained without additional numerical regularization techniques (e.g. arc length method), since there is no unique relation between load and displacement.

In the right representation of Fig. 15, the load–displacement curves of the micropolar material are plotted. The regularization effect of the Cosserat formulation can clearly be observed, i.e. the computations can be carried out on all mesh sizes. Furthermore, the mesh dependence of the solution carried out by use of the standard formulation already vanishes on the medium mesh. Moreover, in comparison of the results computed on the medium

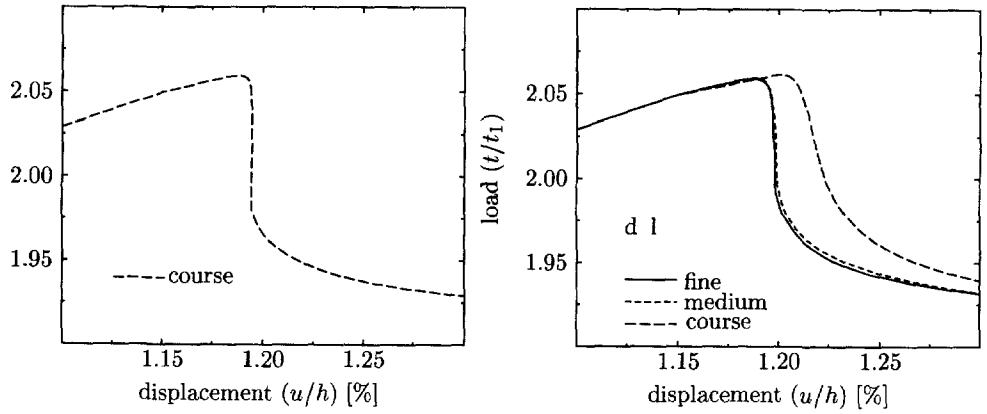

Fig. 15. Load–displacement curves: (left) non-polar material and (right) micropolar material.

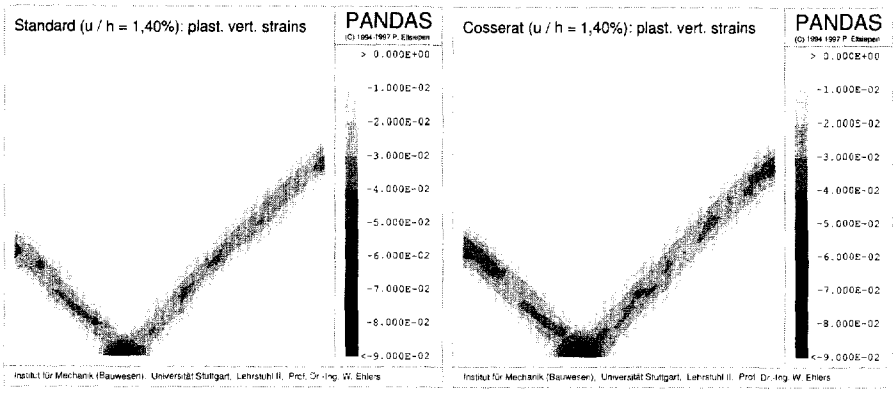

Fig. 16. Numerical biaxial test with weakened area: (left) non-polar material and (right) micropolar material.

and on the fine mesh, it is observed that the shape of the curves is only determined by the Cosserat parameters and not by the spatial discretization.

In Fig. 16, the plastic vertical strain computed on the course mesh is plotted for the standard formulation (left) and for the extended micropolar formulation (right). In comparison of both formulations, the influence of the additional micropolar degrees of freedom governed by the internal length scale parameter l_c obviously leads to a widening of the shear band.

Example 3: *Biaxial test with random distribution of* λ^S

The third example concerns the same biaxial test that has already been discussed in the second example. In order to furthermore clarify the onset and the development of shear bands, the Lamé constant λ^S is randomly distributed over the whole domain within local deviations of $\pm 0.5\%$. In contrast to the above computations, where μ^S and λ^S are weakened in a small domain, thus predicting the point where the localization starts, a random distribution of λ^S does not prescribe the location of the onset of shear banding.

In the framework of the extended micropolar formulation, the computations have been carried out on the medium mesh, compare Fig. 17. When initial plastic yielding occurs (Fig. 17 top left), the plastic deformations are randomly distributed, namely as a result of the random distribution of λ^S. When the loading proceeds (Fig. 17 top right), shear banding starts, and the onset of several shear bands can be observed. After a while, it turns out that there is only one dominant band (Fig. 17 bottom left and bottom right). However, the location of this band cannot be predicted. Since the random distribution of λ^S is responsible for a non-homogeneous problem and thus, for the possibility of shear banding, the final

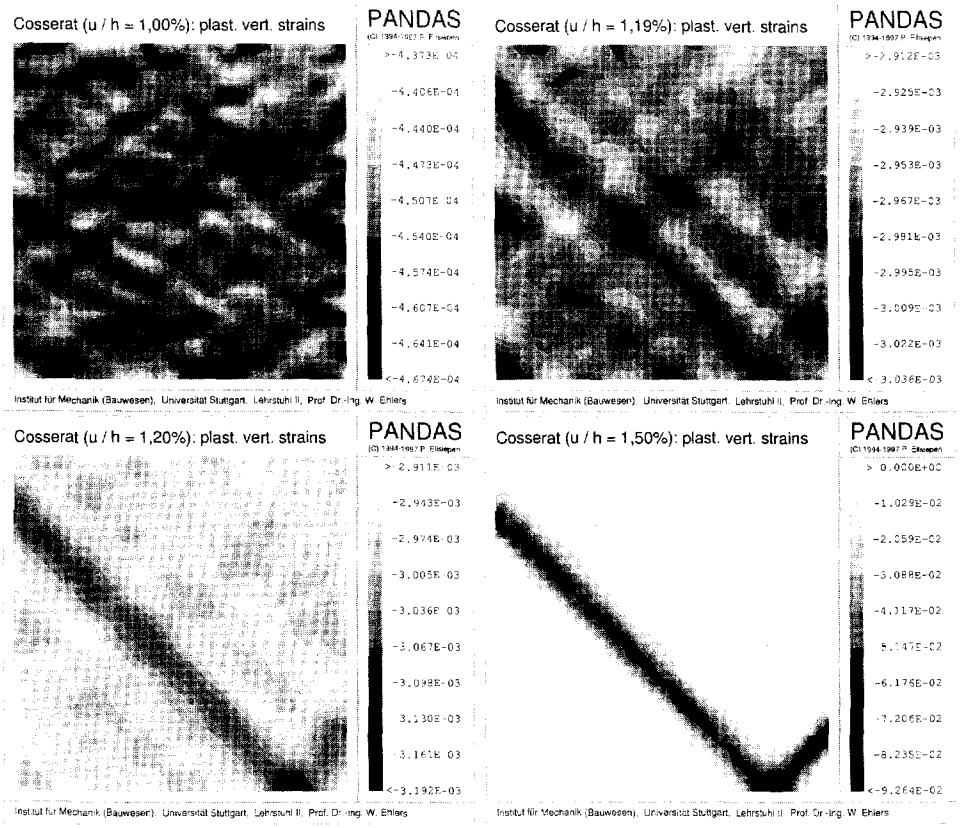

Fig. 17. Numerical biaxial test with random λ^S (Cosserat formulation).

location of the shear band mainly depends on the spatial discretization. As a result, proceeding from a different mesh would obviously lead to a different location of the final dominant shear band.

6. CONCLUDING REMARKS

In the present contribution, non-polar and micropolar elasto-plastic frictional porous solid materials have been studied. In particular, the continuum mechanical results have been applied to localization phenomena, where the regularization of a basically ill-posed problem, as for instance an empty skeleton material described within the standard formulation, could be carried out by the inclusion of additional degrees of freedom in the sense of the Cosserat brothers (extended formulation) and/or by the inclusion of a viscous pore-fluid.

The numerical examples demonstrate the efficiency of the proposed method. In particular, proceeding from the extended micropolar formulation opens the possibility to implicitly include the shear band width into the problem by proposing convenient numbers for the internal length scale parameter. However, since the inclusion of a viscous pore-fluid concerns a different mechanical problem than the description of an empty porous material, regularization by fluid viscosity is clearly restricted to volumetrically coupled saturated problems.

The numerical procedure carried out in the present contribution offers the possibility of describing saturated and empty skeleton materials in the framework of both the standard and the extended formulations.

REFERENCES

Biot, M. A. (1941) General theory of three-dimensional consolidation. *Journal of Applied Physics* **12,** 155–164.

Biot, M. A. (1956) Theory of propagation of elastic waves in a fluid-saturated porous solid, I. Low frequency range. *Journal of Acoustic Society of America* **28,** 168–178.

de Boer, R. (1982) *Vektor- und Tensorrechnung für Ingenieure*. Springer-Verlag, Berlin.
de Boer, R. (1996) Highlights in the historical development of porous media theory: toward a consistent macroscopic theory. *Applied Mechanics Review* **49,** 201–262.
de Boer, R. and Ehlers, W. (1986) *Theorie der Mehrkomponentenkontinua mit Anwendung auf bodenmechanische Probleme*. Forschungsberichte aus dem Fachbereich Bauwesen der Universität-GH-Essen **40,** Essen.
de Boer, R. and Ehlers, W. (1990) The development of the concept of effective stresses. *Acta Mech.* **83,** 77–94.
de Boer, R., Ehlers, W., Kowalski, S. and Plischka, J. (1991) *Porous Media—A Survey of Different Approaches*. Forschungsberichte aus dem Fachbereich Bauwesen der Universität-GH-Essen **54,** Essen.
de Borst, R. (1991) Numerical modelling of bifurcation and localisation in cohesive–frictional materials. *Pageoph.* **137,** 368–390.
de Borst, R. (1993) A generalisation of J_2-flow theory for polar continua. *Comput. Methods Appl. Mech. Engrg* **103,** 347–362.
Bowen, R. M. (1976) Theory of mixtures. In *Continuum Physics*, ed. A. C. Eringen, Vol. III, pp. 1–127. Academic Press, New York.
Bowen, R. M. (1980) Incompressible porous media models by use of the theory of mixtures. *International Journal of Engineering Science* **18,** 1129–1148.
Bowen, R. M. (1982) Compressible porous media models by use of the theory of mixtures. *International Journal of Engineering Science* **20,** 697–735.
Coussy, O. (1995) *Mechanics of Porous Continua*. Wiley, Chichester.
Diebels, S. and Ehlers, W. (1996) On basic equations of multiphase micropolar materials. *Technische Mechanik* **16,** 77–88.
Ehlers, W. (1989) *Poröse Medien—ein kontinuumsmechanisches Modell auf der Basis der Mischungstheorie*. Forschungsberichte aus dem Fachbereich Bauwesen der Universität-GH-Essen **47,** Essen.
Ehlers, W. (1993a) Constitutive equations for granular materials in geomechanical context. In *Continuum Mechanics in Environmental Sciences and Geophysics*, ed. K. Hutter, pp. 313–402. CISM Courses and Lecture Notes No. 337. Springer-Verlag, Wien.
Ehlers, W. (1993b) Compressible, incompressible and hybrid two-phase models in porous media theories. *ASME: AMD-Vol.* **158,** 25–38.
Ehlers, W. (1995) A single surface yield function for geomaterials. *Arch. Appl. Mech.* **65,** 246–259.
Ehlers, W. (1996) Grundlegende Konzepte in der Theorie Poröser Medien. *Technische Mechanik* **16,** 63–76.
Ehlers, W. and Kubik, J. (1994) On finite dynamic equations for fluid-saturated porous media. *Acta Mechanica* **105,** 101–117.
Ehlers, W. and Volk, W. (1997a) On shear band localization phenomena of liquid-saturated granular elasto-plastic porous solid materials accounting for fluid viscosity and micropolar solid rotations. *Mech. Cohesive-frictional Mater.* **2,** 301–320.
Ehlers, W. and Volk, W. (1997b) On shear band localization phenomena induced by elasto-plastic consolidation of fluid-saturated soils. In *Computational Plasticity—Fundamentals and Applications*, ed. D. J. R. Owen, E. Oñate and E. Hinton, Vol. 2, pp. 1657–1664. CIMNE, Barcelona.
Ehlers, W. and Volk, W. (1997c) Localization phenomena in liquid-saturated soils. In *Proceedings of NAFEMS World Congress '97*, ed. A. Creechan *et al.*, Vol. 1, pp. 287–298. Bell and Bain, Glasgow.
Ehlers, W., Diebels, S. and Mahnkopf, D. (1995) Elasto-plastic consolidation of fluid-saturated soils. In *Computational Plasticity—Fundamentals and Applications*, ed. D. J. R. Owen, E. Oñate and E. Hinton, Vol. 2, pp. 1689–1700. Pineridge Press, Swansea.
Haupt, P. (1993) Foundations of continuum mechanics. In *Continuum Mechanics in Environmental Sciences and Geophysics*, ed. K. Hutter, pp. 1–77. CISM Courses and Lecture Notes No. 337. Springer-Verlag, Wien.
Lade, P. V. and Duncan, J. M. (1973) Cubical triaxial tests on cohesionless soils. *ASME: J. Soil Mech. Found. Div.* **99,** 793–812.
Nowacki, W. (1986) *Theory of Asymmetric Elasticity*. Pergamon Press, Oxford.
Schad, H. (1979) *Nichtlineare Stoffgleichungen für Böden und ihre Verwendung bei der numerischen Analyse von Grundbauaufgaben*. Mitteilungen des Baugrundinstituts der Universität Stuttgart **10,** Stuttgart.
Steinmann, P. (1994) A micropolar theory of finite deformation and finite rotation multiplicative elastoplasticity. *International Journal of Solids and Structures* **31,** 1063–1084.
Steinmann, P. (1995) Theory and numerics of ductile micropolar elastoplastic damage. *International Journal of Numerical Methods in Engineering* **38,** 583–606.
Terzaghi, K. (1923) Die Berechnung der Durchlässigkeitsziffer des Tones aus dem Verlauf der hydrodynamischen Spannungserscheinungen. *Sitzungsber. Akad. Wiss. (Wien), Math.-Naturwiss. Klasse*, Abt. IIa **132,** 125–138.
Terzaghi, K. and Jelinek, R. (1954) *Theoretische Bodenmechanik*. Springer-Verlag, Berlin.
Truesdell, C. and Toupin, R.A. (1960) The classical field theories. In *Handbuch der Physik*, Band III/1, ed. S. Flügge, pp. 226–902. Springer-Verlag, Berlin.